

Supporting Information

Switching of Light Responsive Metal–Organic Gels from Insulator to Semiconductor: Flexible Smart Semiconducting Membranes for Optoelectronic Device Fabrication

Mouli Das Dawn,^[a] Someprosad Patra,^[b] Debamalya Banerjee,^[b] and Kumar Biradha*^[a]

[a] Department of Chemistry, Indian Institute of Technology Kharagpur
Kharagpur 721302, India

E-mail: kbiradha@chem.iitkgp.ac.in.

Fax: +91-3222- 282252. Tel.: +91-3222-283346.

[b] Department of Physics, Indian Institute of Technology Kharagpur
Kharagpur 721302, India

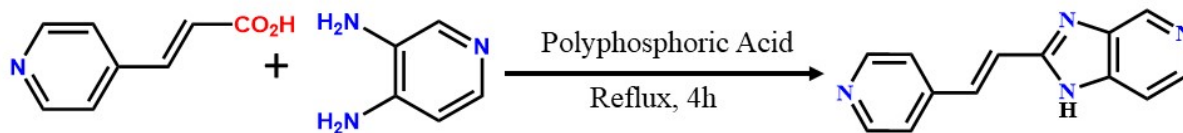
Contents

1.	Section S1	General aspects
2.	Section S2	Synthesis of ligand
3.	Section S3	Gelation and rheology
4.	Section S4	Characterization of MOG
5.	Section S5	Photochemical reaction of MOG
6.	Section S6	Characterization after metal salt doping
7	Section S7	Conductivity measurement of the Pellet
8.	Section S8	Characterization of the device on ITO glass and conductivity measurement
9.	Section S9	Characterization of Mixed-matrix membrane and conductivity measurement
10.	Section S10	Comparison Table

All the chemicals, and solvents such as pyridine, Malonic acid, 4-Pyridine Aldehyde, Piperidine, 3,4-Diamino Pyridine, Polyphosphoric acid, Ammonia solution, Methanol, Nickel(II) acetate tetrahydrate, Lithium nitrate, Magnesium nitrate hexahydrate, Aluminium nitrate nonahydrate, Polyvinylpyrrolidone, Poly(vinylidene fluoride), DMF, Isopropanol, Acetone were purchased from local chemical suppliers and used without further purification.

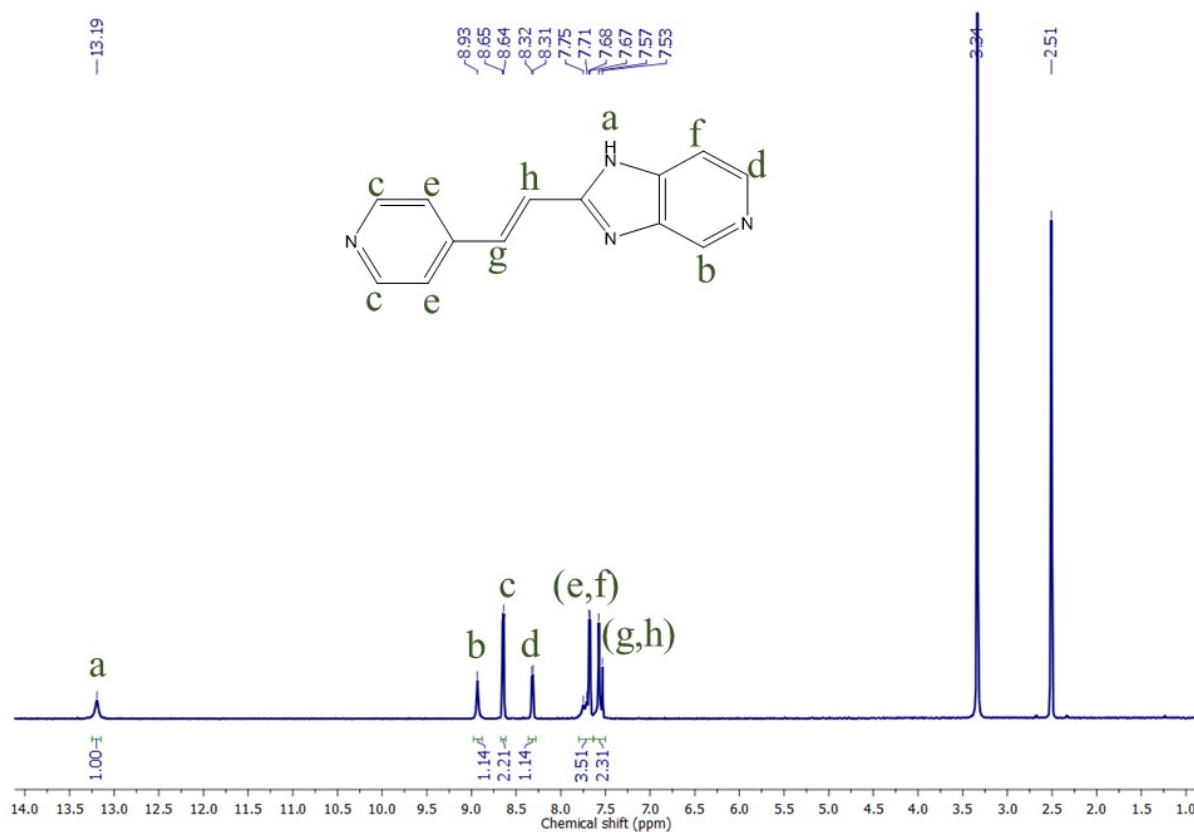
Rheological measurements were carried out on an Anton Paar MCR 102 rheometer using a 25 mm diameter parallel plate geometry with a constant tool gap of 1 mm. The PXRD patterns were recorded with a BRUKER-AXS-D8-ADVANCE diffractometer at room temperature. ¹H NMR spectra were recorded on a Bruker 500 MHz NMR instrument. Perkin-Elmer, UATR Two spectrometer was used to record the FTIR spectra. Field-emission scanning electron microscopy (FESEM) was performed on a ZEISS VP 300 instrument with an Oxford EDS detector, operated at an accelerating voltage of 5–10 kV. Transmission Electron Microscopy (TEM) analysis performed by JEM-ARM 200F (NEO ARM) operated at an acceleration voltage from 30 to 200 kV. Mechanical properties of the membranes were tested in Tinius Olsen H50KS Universal Testing Machine at room temperature. Nanoindentation studies were carried out with Hysitron TI950 TriboIndenter. The diffuse reflectance spectra (DRS) were recorded with a Cary model 5000 UV–visible–NIR spectrophotometer. Raman spectroscopic measurements were carried out at room temperature by using a T64000 (JY, France) micro-Raman spectrometer with an excitation wavelength of 532 nm. X-ray photoelectron spectroscopy (XPS) was performed in an ESCALAB Xi, Thermo-Scientific, UK, having a monochromatic Al K α X-ray source (1486.6 eV). The CAE (constant analyzer energy) for survey spectra is 100 eV and that for high-resolution spectra is 50 eV. Electrical conductivity measurements were performed by using the two-probe direct current method with a Keithley 2450 source measure unit instrument at 298 K.

Section S2 **Synthesis of Ligand**



Scheme S1. Ligand (L) synthesis

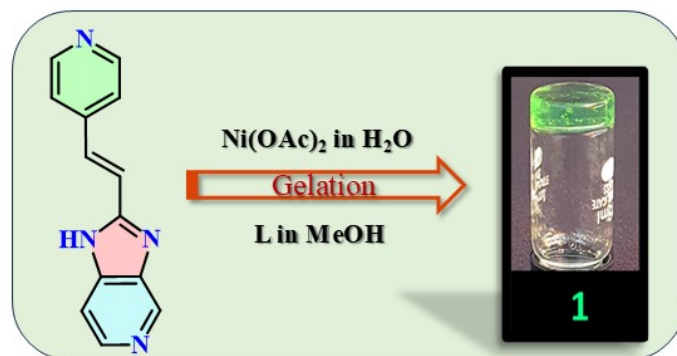
¹H-NMR spectrum of Ligand (L)



Section S3

Gelation and Rheology

The addition of methanolic solutions (1ml) of L (0.022 g, 0.1 mmol) into aqueous solution (1ml) of Nickel(II) acetate tetrahydrate (0.0248 g, 0.1 mmol) resulted in the formation of green gelatinous type of material (1) in room temperature.



Scheme S1. Formation of photoreactive Ni-MOG (1)

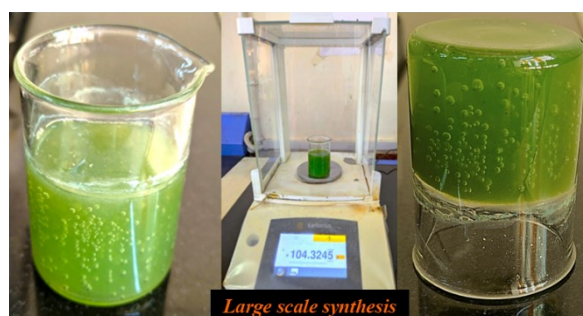


Fig. S1: Large-scale Ni-MOG (1) synthesis.

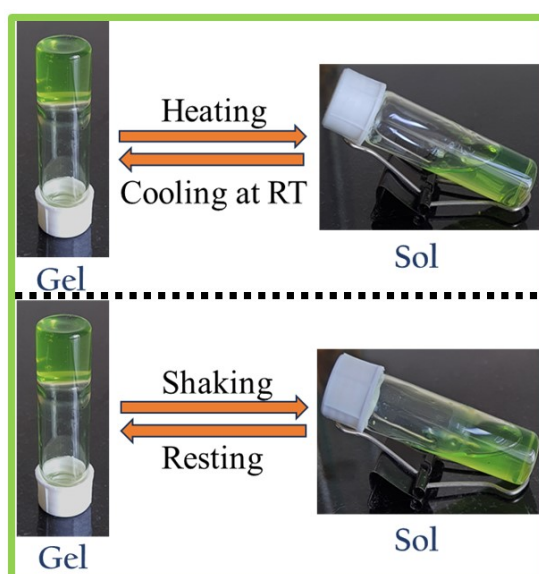


Fig. S2: Thermoreversible and thixotropic behaviour of 1.

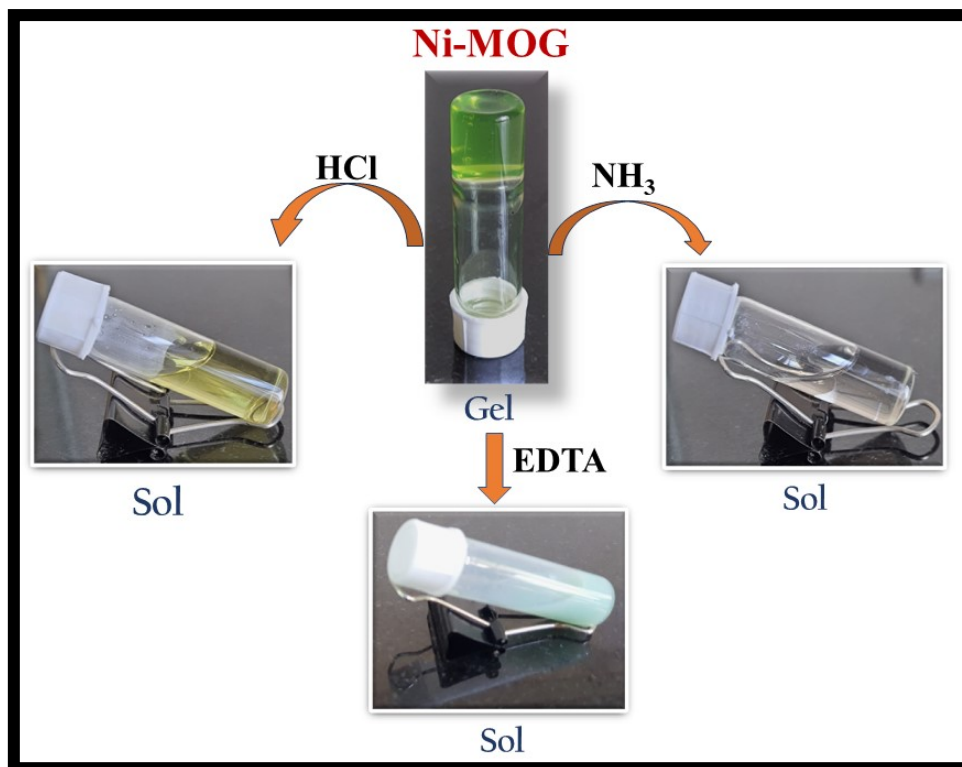


Fig. S3. Illustration for gel-sol transformation of **1** by adding external chemical stimuli.

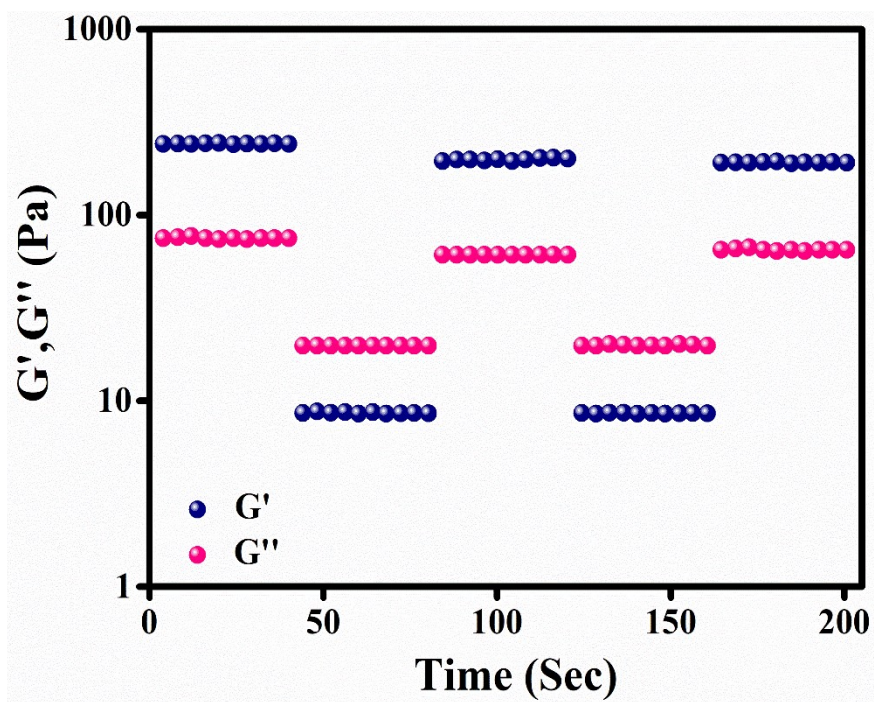


Fig. S4. A step-strain experiment at a constant frequency of 10 rad s^{-1} of **1**.



Fig. S5. Gel formation in Ethanol and Propanol.

Table S1: Rheological data in different aliphatic alcoholic solvents.

Solvent system	Gel formation	Inverted vial test	Rheology data	
			G', G'' (Pa)	Yield stress (Pa)
Methanol	Yes	Yes	5885	17
Ethanol	Yes	Yes	607.26	13.68
Propanol	Yes	Yes	429.68	9.05
Butanol	No	No	-	-
Hexanol	No	No	-	-
Heptanol	No	No	-	-
Octanol	No	No	-	-
Decanol	No	No	-	-

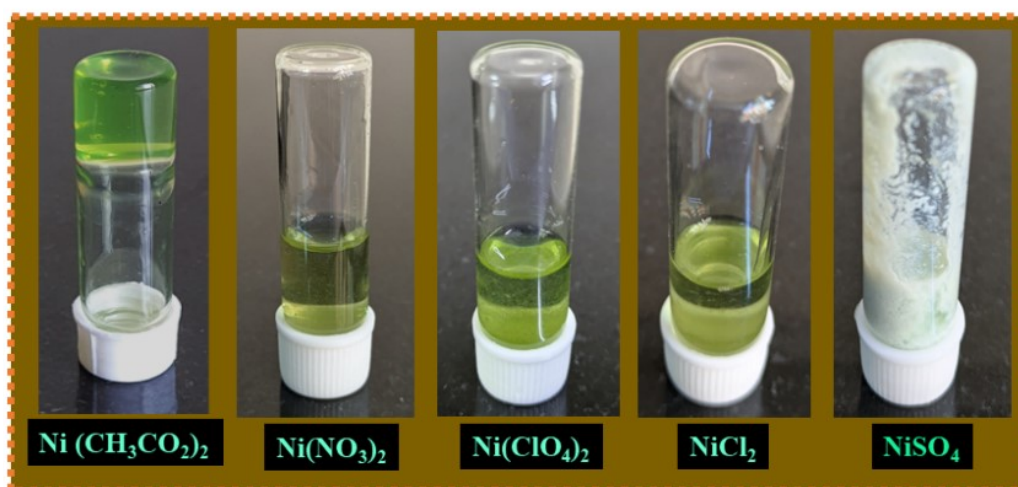


Fig. S6.: Gel formation trial with various Nickel salts.

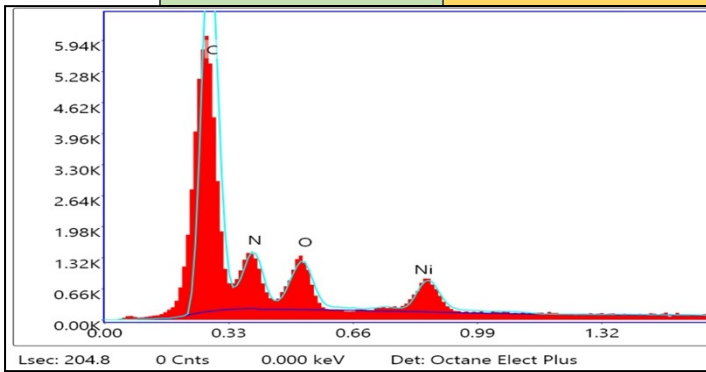
Section S4**Characterization of MOG**

Fig. S7 EDAX analysis of 1.

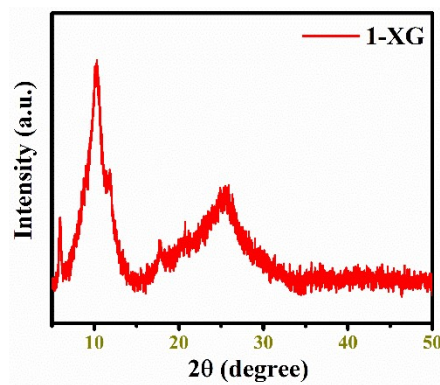


Fig. S8. PXRD pattern of 1-XG.

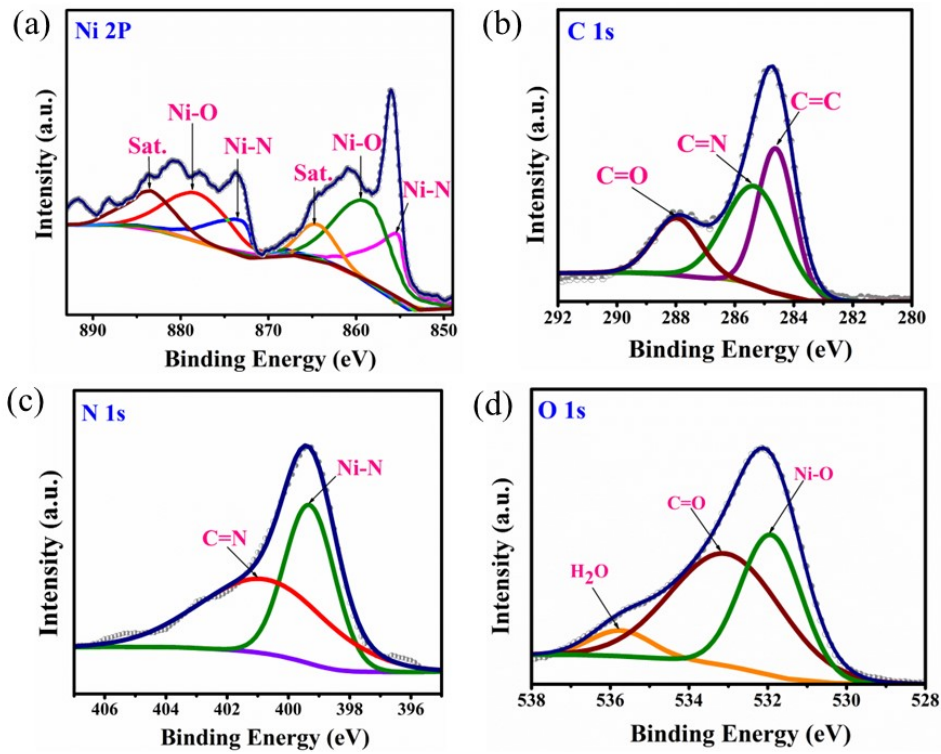


Fig. S9. XPS spectra of the 1-XG (a) high-resolution Ni 2p. (b) C 1s (c) N 1s (d) O 1s.

Section S5**Photochemical reaction of MOG**

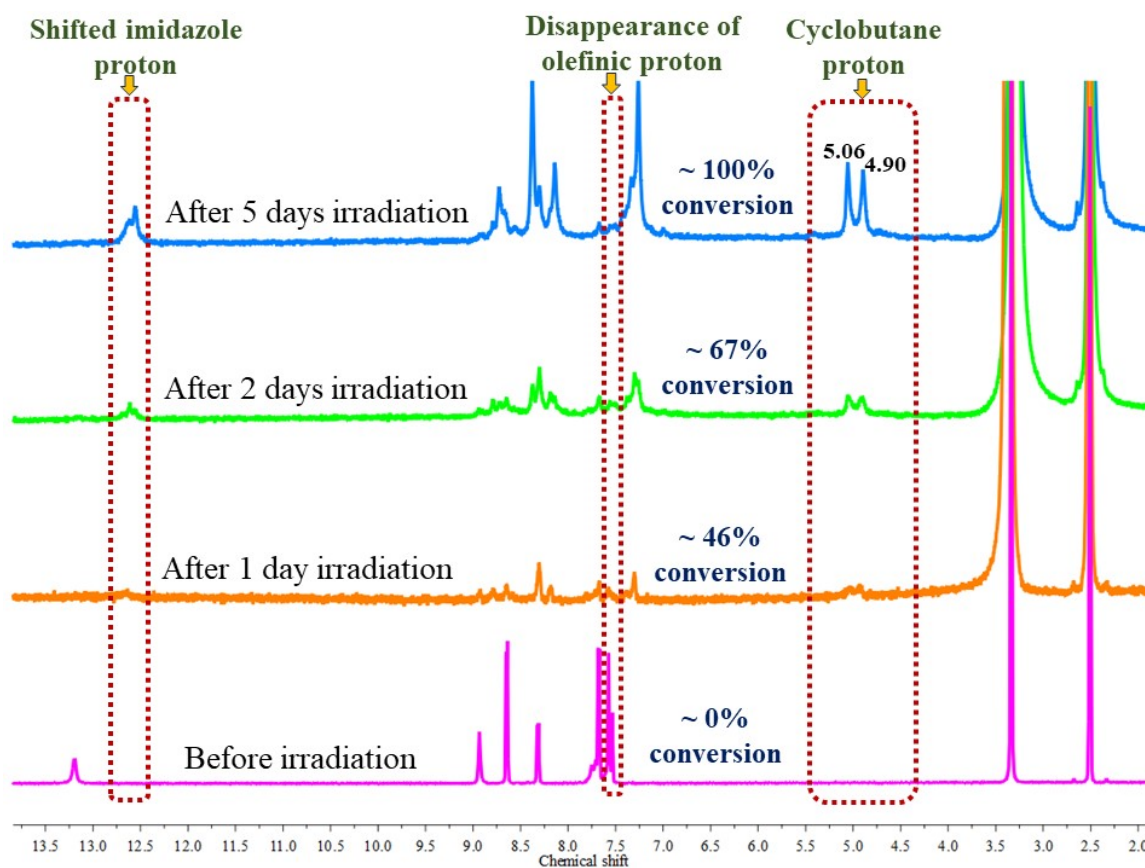


Fig. S10. ^1H NMR spectra of **1** in DMSO-d_6 at different time-intervals of irradiation in UV-A.

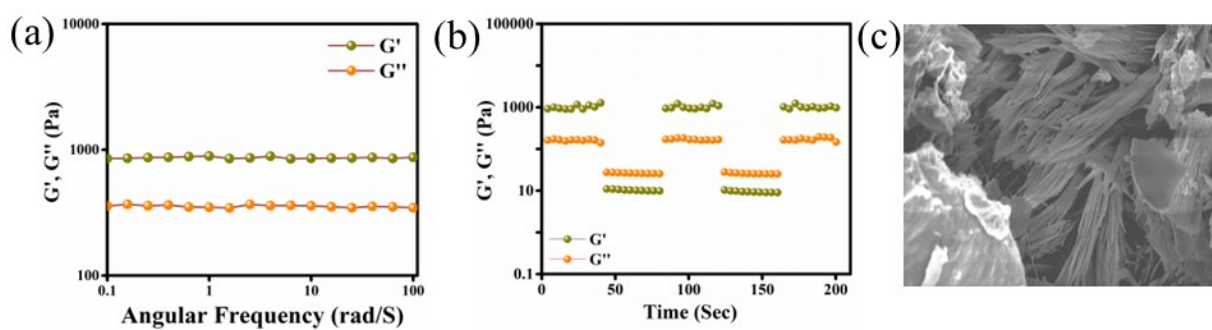


Fig. S11. (a) Variation of storage modulus (G') and loss modulus (G'') with the frequency of **1**'; (b) A step-strain experiment at a constant frequency of 10 rad s^{-1} of **1**'; (c) FESEM image of **1**'.

Synthesis of 1@M and 1'@M: To investigate the performance of metal doping in gel, **1** and **1'** were soaked into a 1M methanolic solution of metal nitrate ($\text{LiNO}_3/\text{Mg}(\text{NO}_3)_2$) for about 48 hrs. The resulting material was washed thoroughly with a methanol solution. ICP-MS analysis indicated the percentage uptake of Li and Mg content in each material.

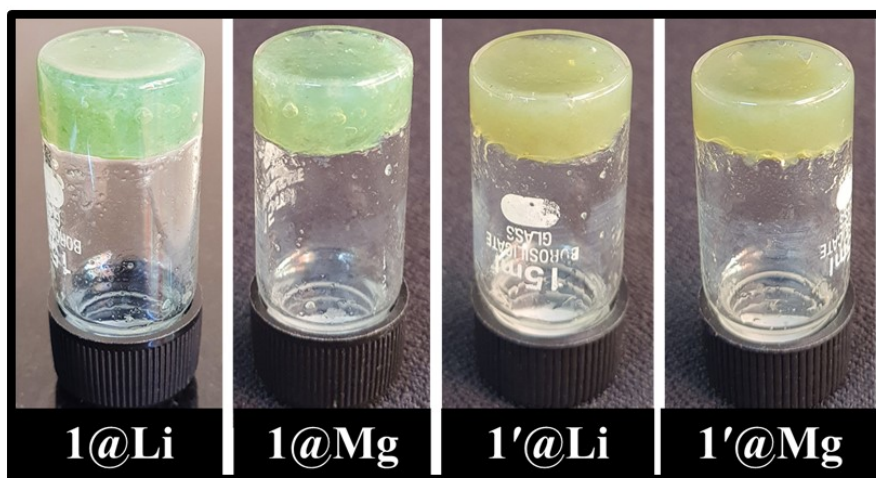


Fig. S12. Inverted vial test after metal salt doping in **1** and **1'**.

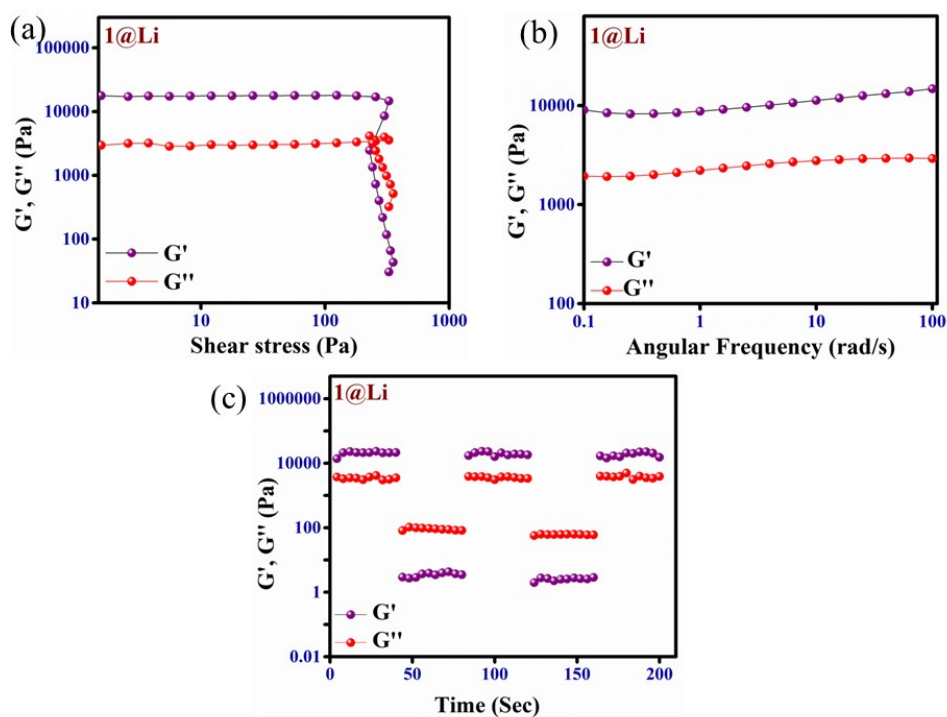


Fig. S13. Rheological data of **1@Li** (a) Variation of storage modulus (G') and loss modulus (G'') with shear stress; (b) Variation of storage modulus (G') and loss modulus (G'') with frequency; (c) with a step-strain experiment at a constant frequency of 10 rad s^{-1} .

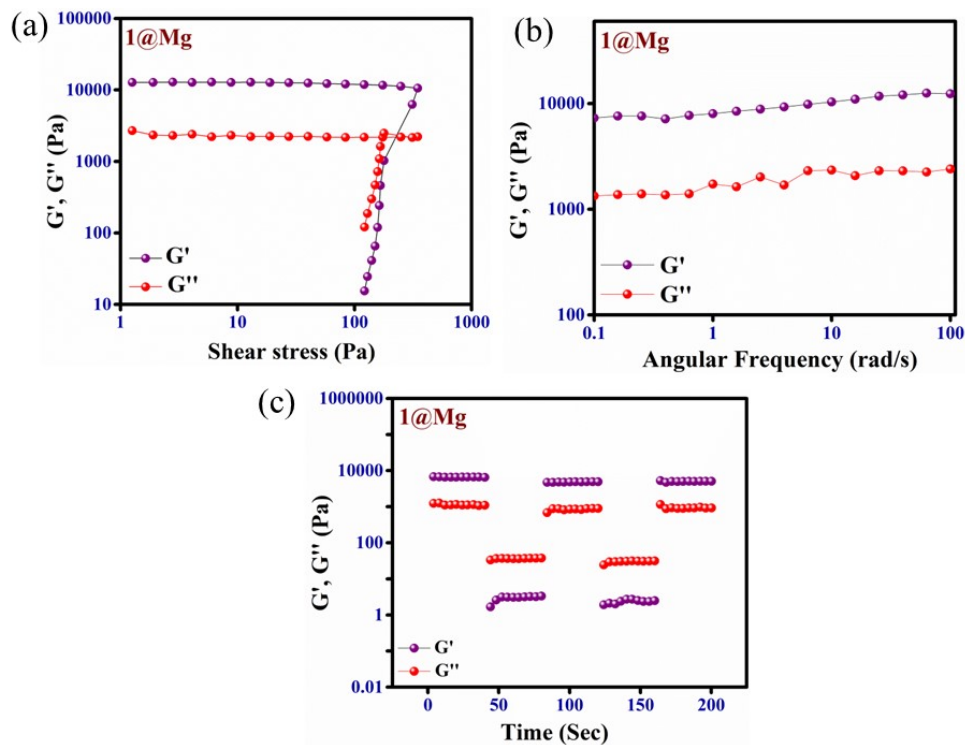


Fig. S14. Rheological data of 1@Mg (a) Variation of storage modulus (G') and loss modulus (G'') with shear stress; (b) Variation of storage modulus (G') and loss modulus (G'') with frequency; (c) with a step-strain experiment at a constant frequency of 10 rad s^{-1} .

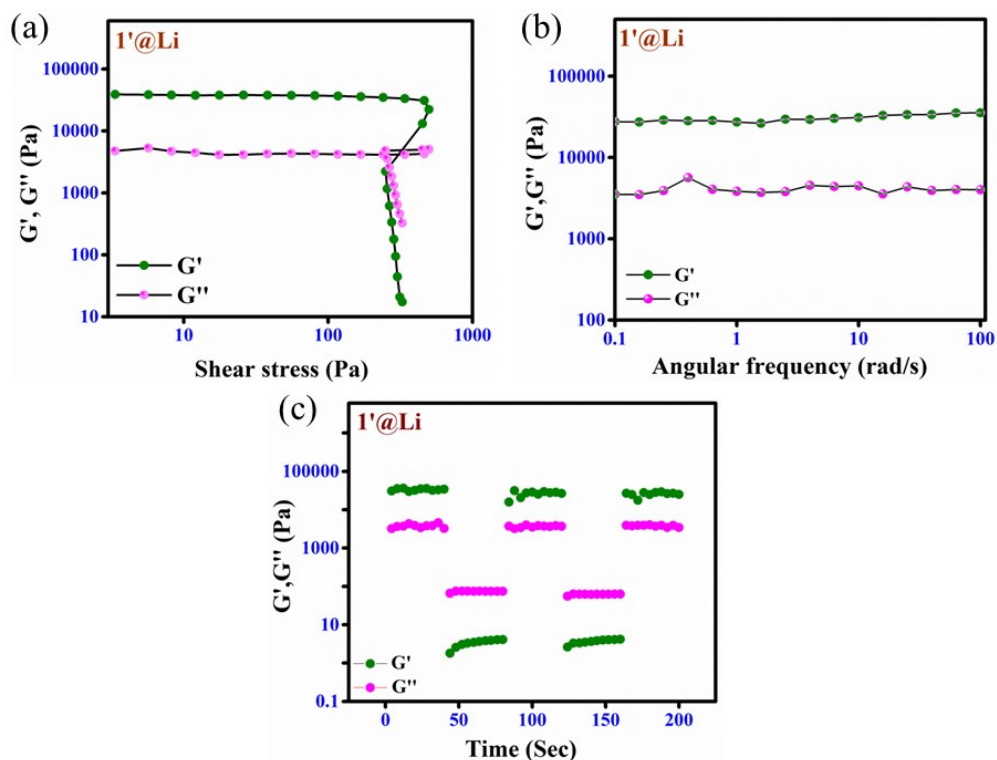


Fig. S15. Rheological data of 1'@Li (a) Variation of storage modulus (G') and loss modulus (G'') with shear stress; (b) Variation of storage modulus (G') and loss modulus (G'') with frequency; (c) with a step-strain experiment at a constant frequency of 10 rad s^{-1} .

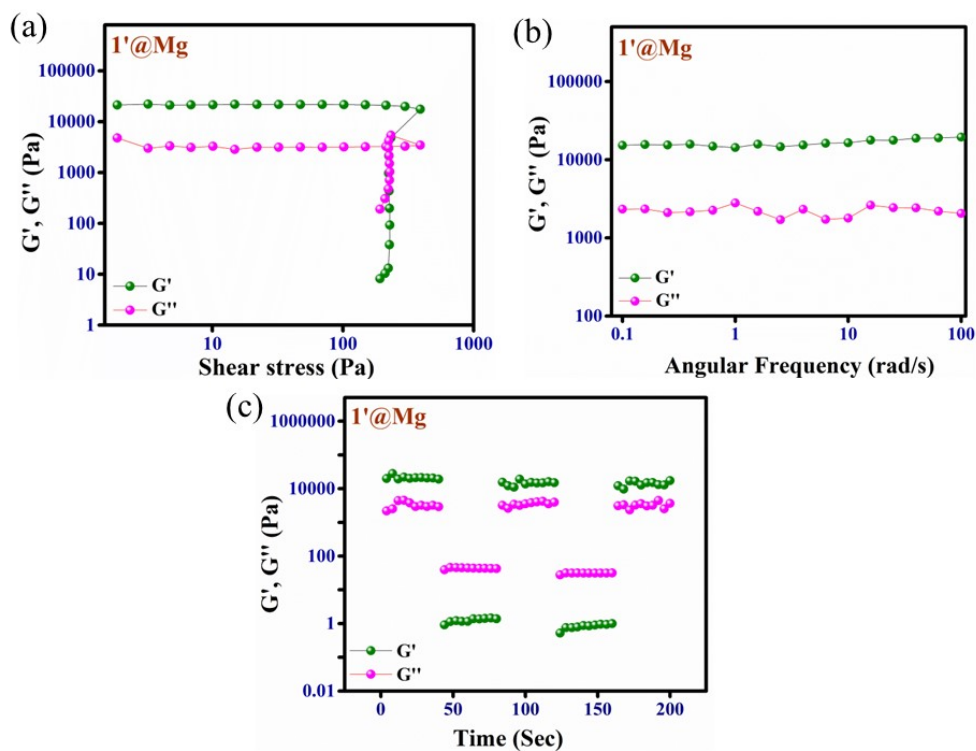


Fig. S16. Rheological data of $1'@Mg$ (a) Variation of storage modulus (G') and loss modulus (G'') with shear stress; (b) Variation of storage modulus (G') and loss modulus (G'') with frequency; (c) with a step-strain experiment at a constant frequency of 10 rad s^{-1} .

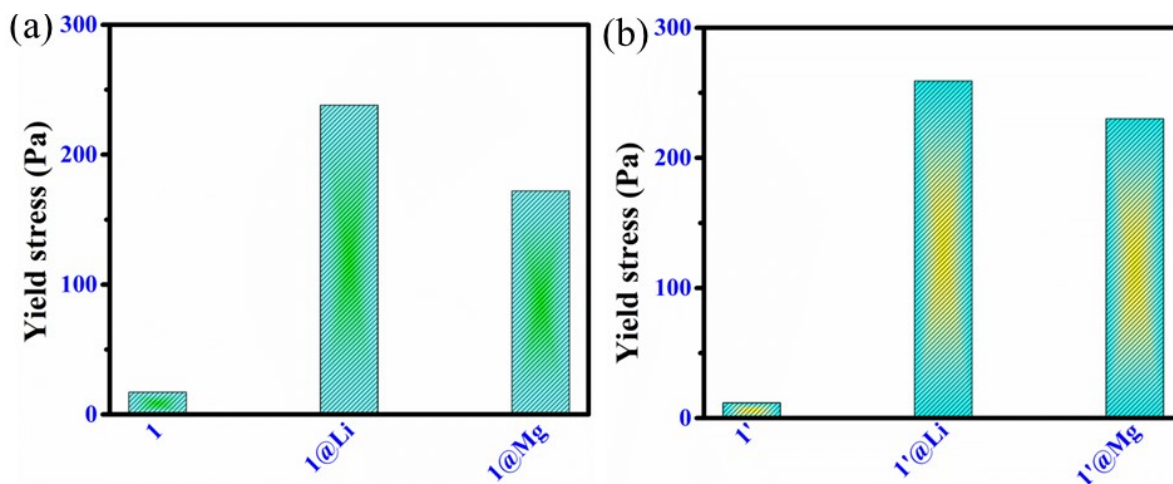


Fig. S17. Comparison of gel strength before and after uptake of Li^+ and Mg^{2+} in (a) 1 and (b) $1'$.

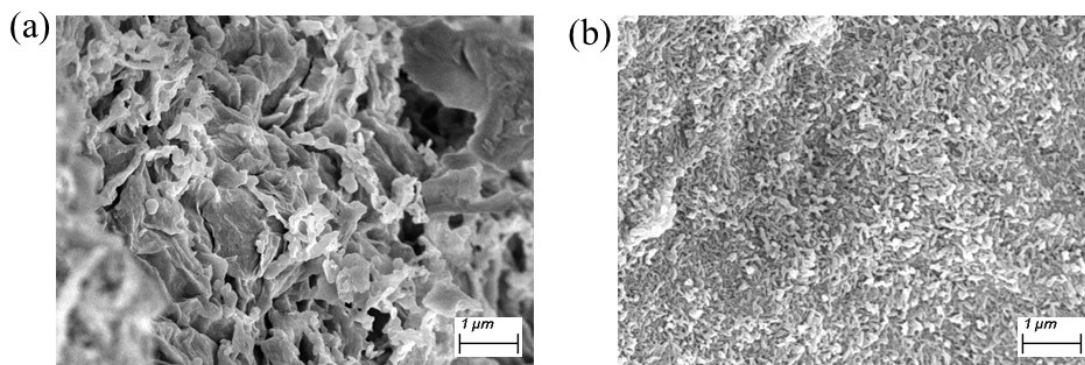


Fig. S18. FESEM image of (a) 1@Li and (b) 1@Mg.

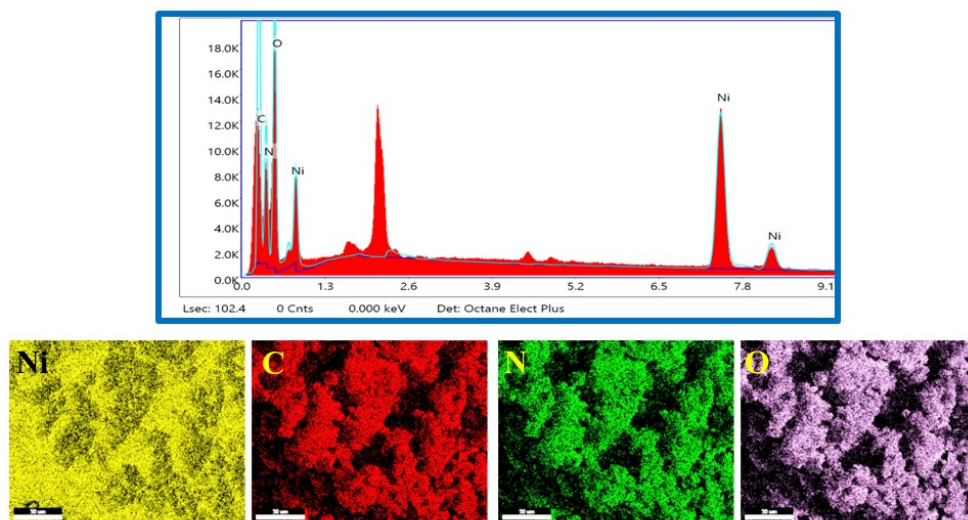


Fig. S19. EDAX and elemental analysis of 1@Li.

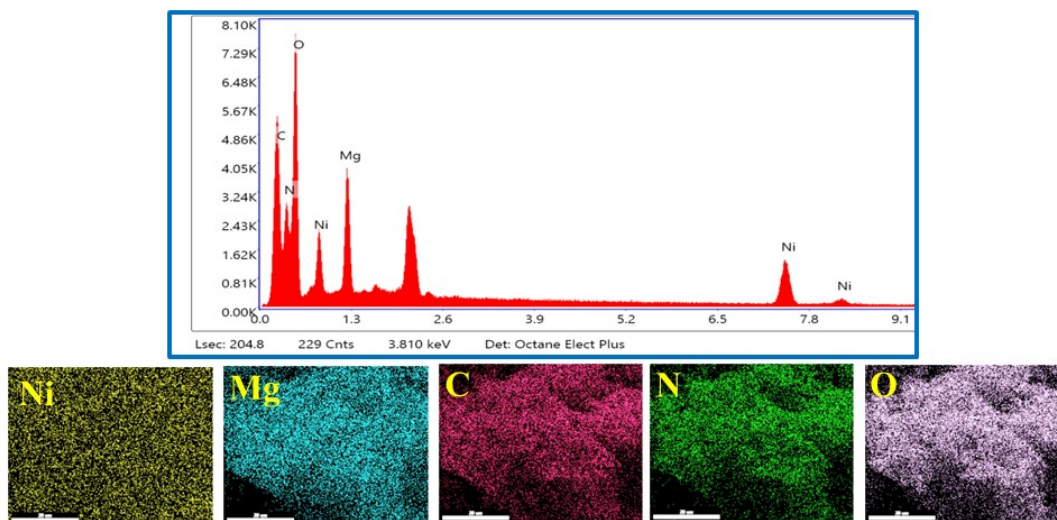


Fig. S20. EDAX and elemental analysis of 1@Mg.

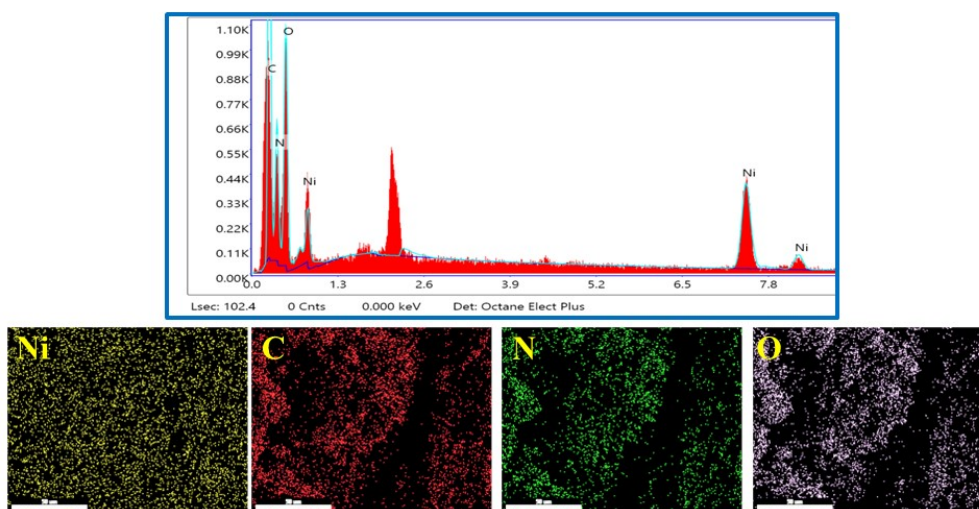


Fig. S21. EDAX and elemental analysis of 1'@Li.

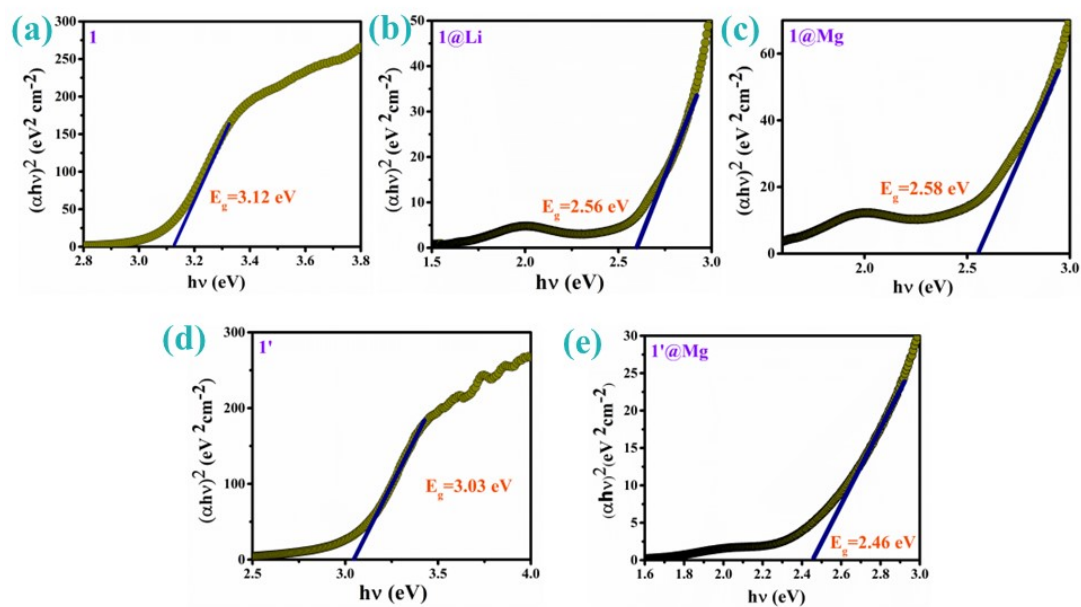


Fig. S22. Tauc's plot of (a) 1 (b) 1@Li (c) 1@Mg (d) 1' (e) 1'@Mg.

Section S7

Conductivity measurement of the pellet

Electrical conductivity measurements were performed by using two-probe direct current method with a Keithley 2450 source measure unit instrument at 298 K. Before constructing the experiment, the pellet sample was prepared using 10 mm die set in hydraulic press machine.

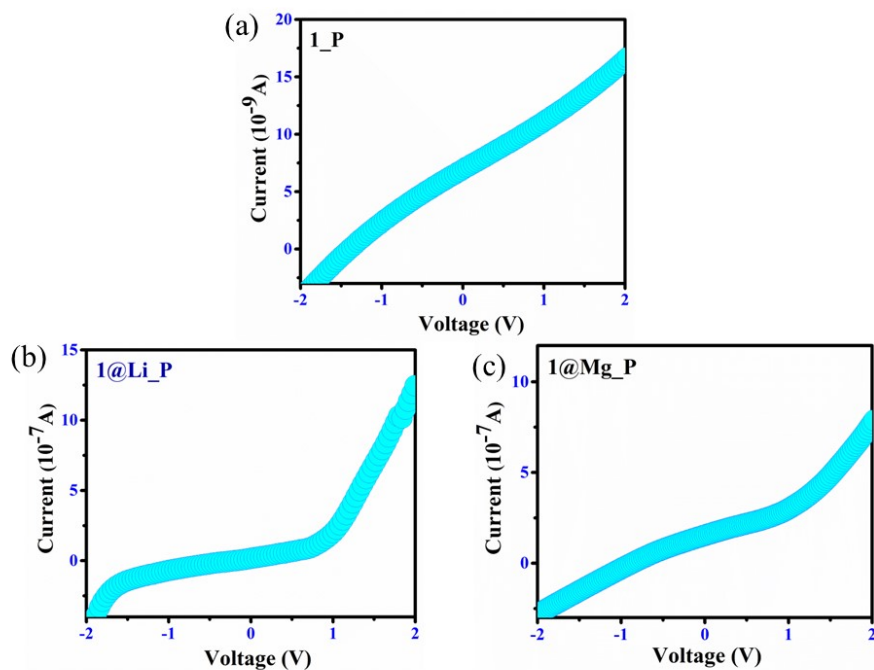


Fig. S23. Current-Voltage (I-V) plots for (a) 1_P (b) 1@Li_P (c) 1@Mg_P.

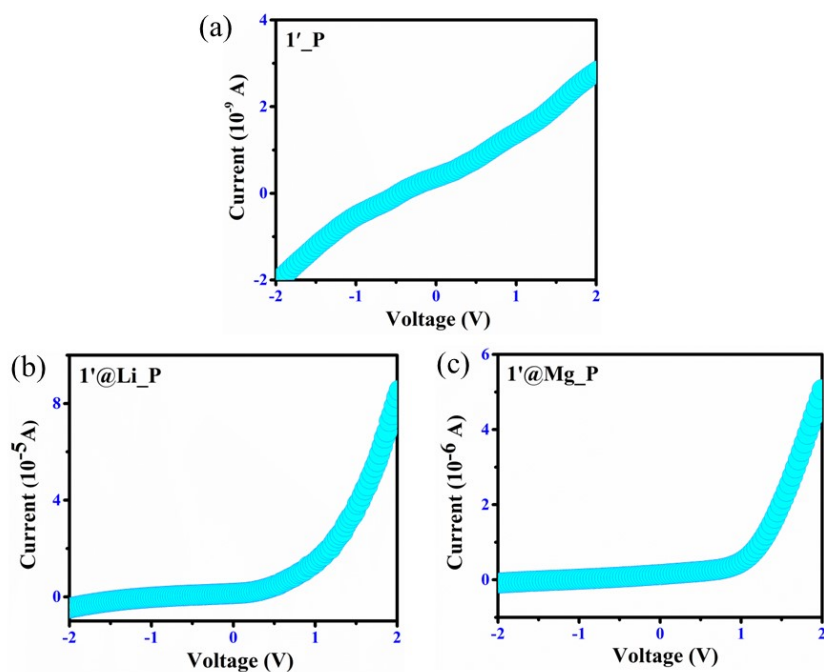


Fig. S24. Current-Voltage (I-V) plots for (a) 1'_P (b) 1'@Li_P (c) 1'@Mg_P.

Section S8 Characterization of device on ITO glass and conductivity measurement

To fabricate the device, at first, Indium Tin Oxide (ITO) coated glass substrate was cleaned by acetone, distilled water, and isopropanol repeatedly and sequentially in an ultrasonication bath for 1 hr. After that, the cleaning performed by the microwave plasma cleaner. Prepared MOG was spin coated onto the pre-cleaned ITO coated glass with the help of a spin coater. This spin coating step was repeated 3 times. After that film was drying in the vacuum. Finally, Aluminum (Al) electrodes were deposited onto the film by a Vacuum Coating under a pressure of 10^{-6} mbar. The effected area of the film was maintained as $7.065 \times 10^{-6} \text{ m}^2$. The current-voltage measurements of the fabricated device were carried out by a Keithley 2450 source meter interfaced by two-probe technique at room temperature.



Fig. S25. Stepwise Thin-film preparation process step-1: cleaning by acetone, water, and isopropanol sequentially; step-2: cleaning by microwave plasma cleaner; step-3: putting sample for spin coating; step-4: Spin-coating; step-5: Spin-coated sample dried in vacuum for measurement.

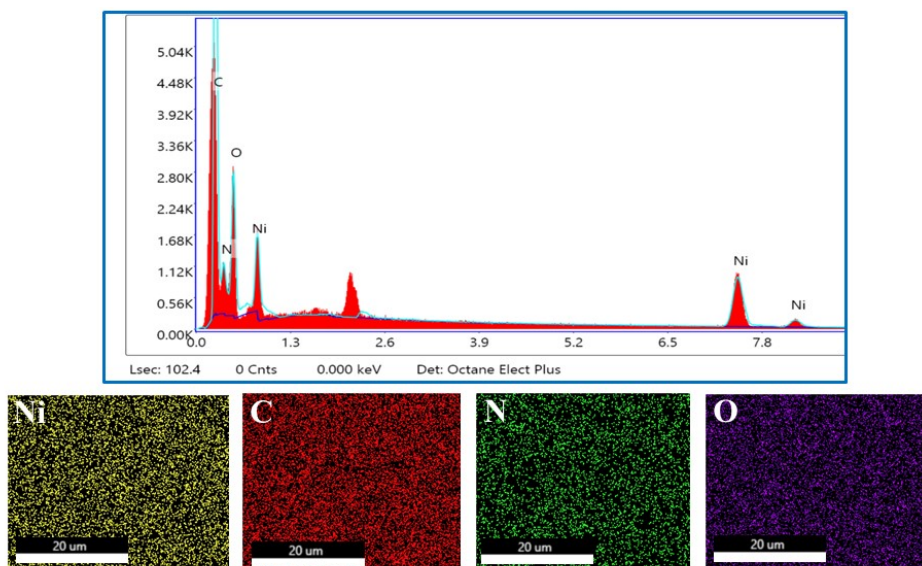


Fig. S26. EDAX and elemental mapping of 1@Li_T

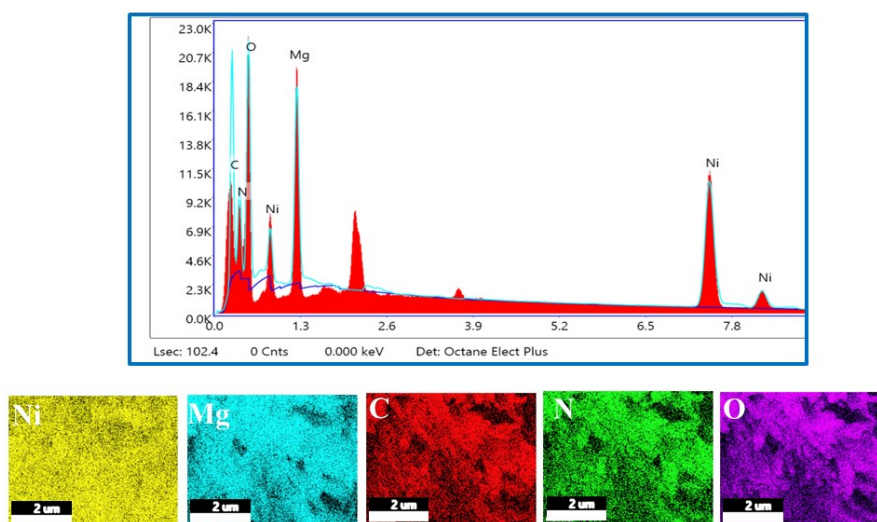


Fig. S27. EDAX and elemental mapping of 1@Mg_T.

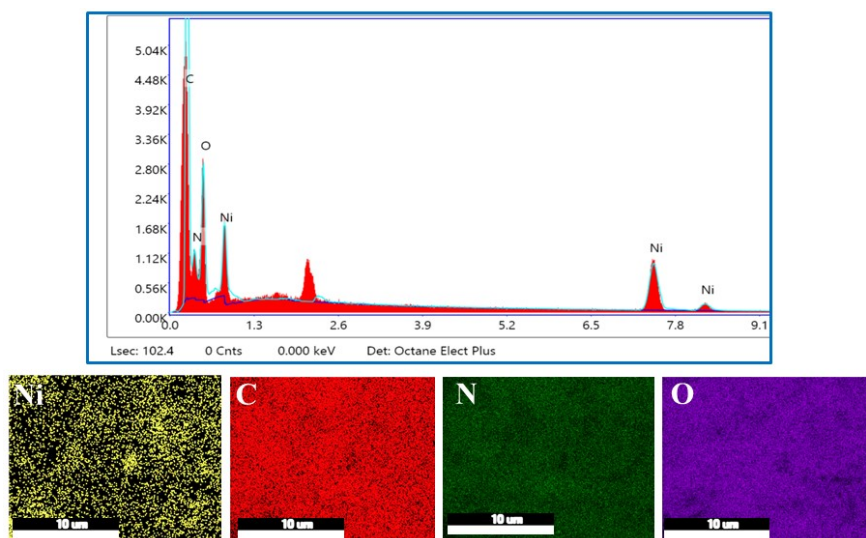


Fig. S28. EDAX and elemental mapping of 1'@Li_T.

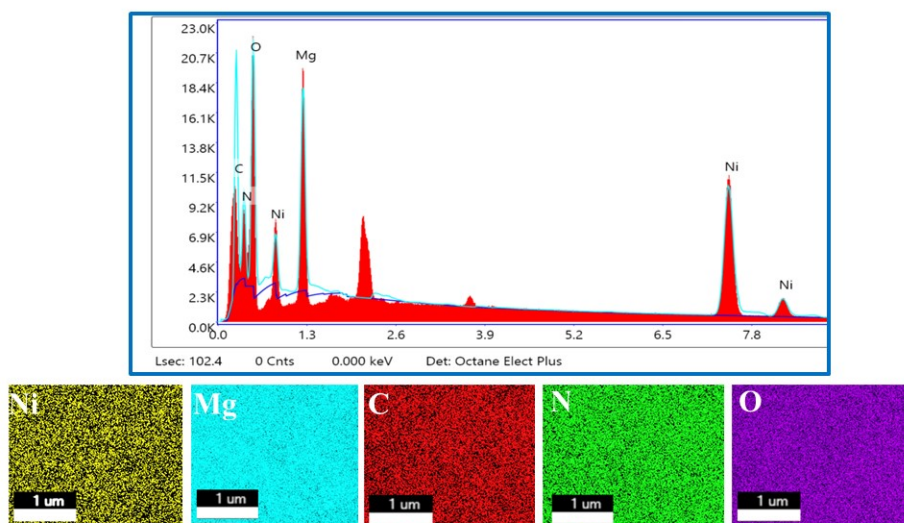


Fig. S29. EDAX and elemental mapping of 1'@Mg_T.

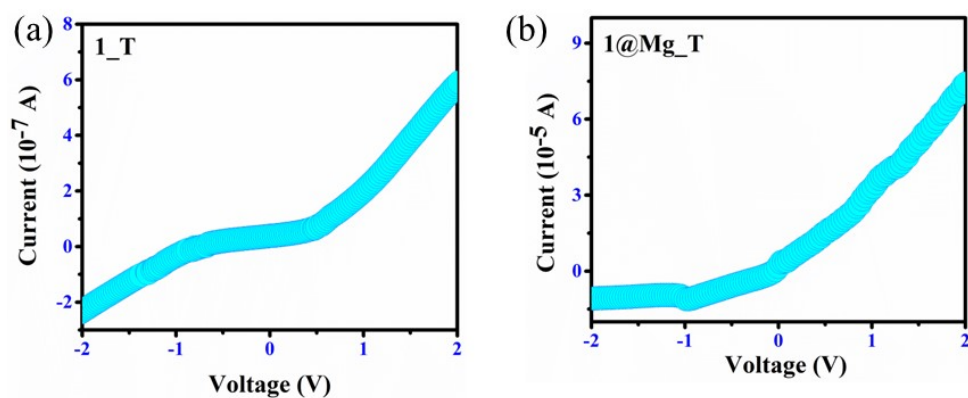


Fig. S30. Current-Voltage (I-V) plots for (a) 1_T (b) 1@Mg_T.

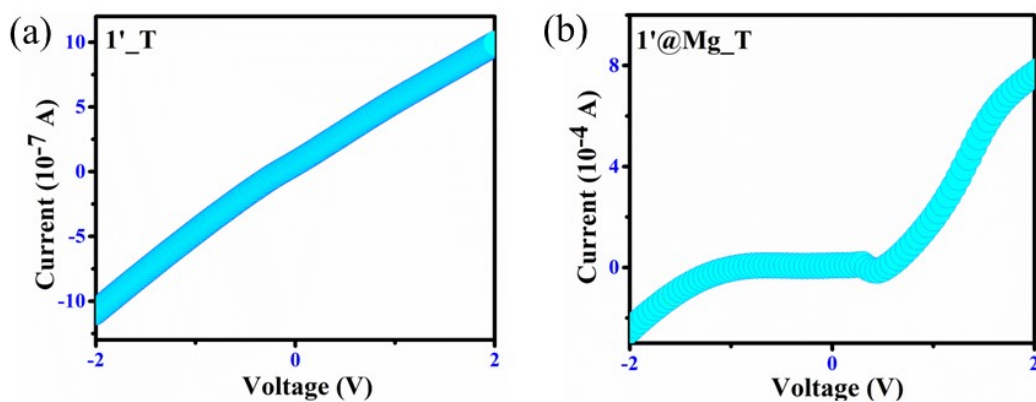


Fig. S31. Current-Voltage (I-V) plots for (a) 1'_T (b) 1'@Mg_T.

In this study, mixed-matrix membranes were fabricated by slurry-casting method. The materials **1**, **1'**, **1@Li**, **1'@Li**, **1@Mg** and **1'@Mg** were mixed with PVP (75 wt %) and PVDF (25 wt %) with varying amounts to prepare membranes **1'@X_M-0**, **1'@X_M-20**, **1'@X_M-40**, and **1'@X_M-60** (0, 20, 40, 60 represents weight percentages of corresponding MOGs, X= Li or Mg and M refers to membrane). All composite membranes were prepared using a similar procedure. In a typical preparation process of **1'@Li_M-60**, 120 mg of **1'@Li** microcrystals were ultrasonically dispersed in DMF (3 mL) for 5 h to produce a suspension. After that, PVDF-PVP (1:3) powders were added to the above suspension and the mixture was stirred at room temperature for 3 h to obtain a homogeneous dispersion. This homogeneous material was poured onto a petri dish, and dried at 80 °C for 6 h to remove DMF. The solidified membrane was removed from the petri dish, and dried at 120 °C under vacuum to eliminate any residual solvents. Electrical conductivity measurements were performed by using the two-probe direct current method with a Keithley 2450 source measure unit instrument at 298 K. In a typical procedure, each membrane of dimension 5 mm x 2 mm x 0.12 mm was utilized for the electrical conductivity measurement.



Fig. S32. Optical image of membrane **1@X_M** (X=Li, Mg) with varying loading percentage.



Fig. S33. Optical image of membrane **1'@X_M** (X=Li, Mg) with varying loading percentage.

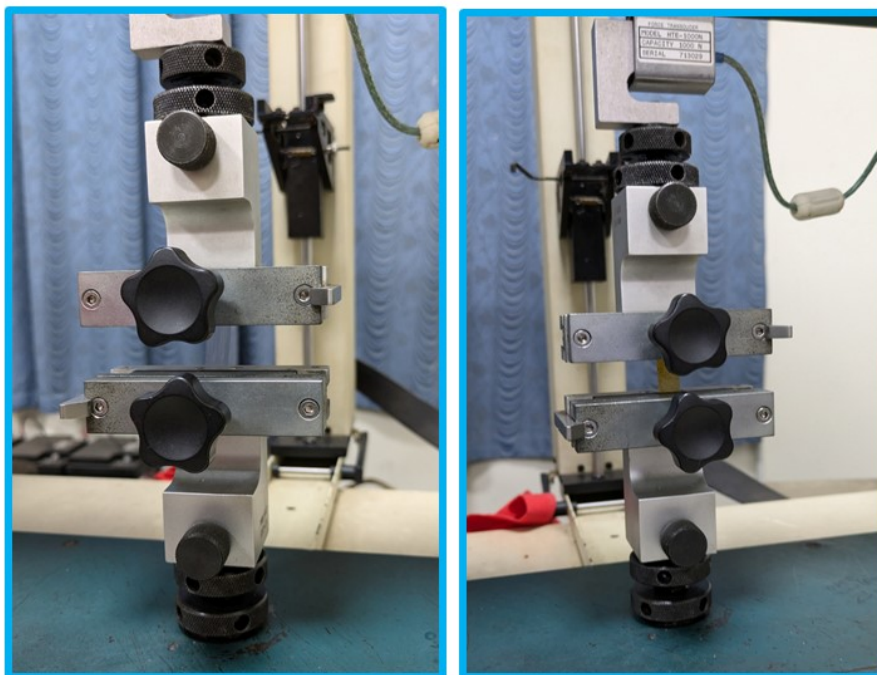


Fig. S34. Study of the mechanical strength of Mixed-matrix membrane (MMM).

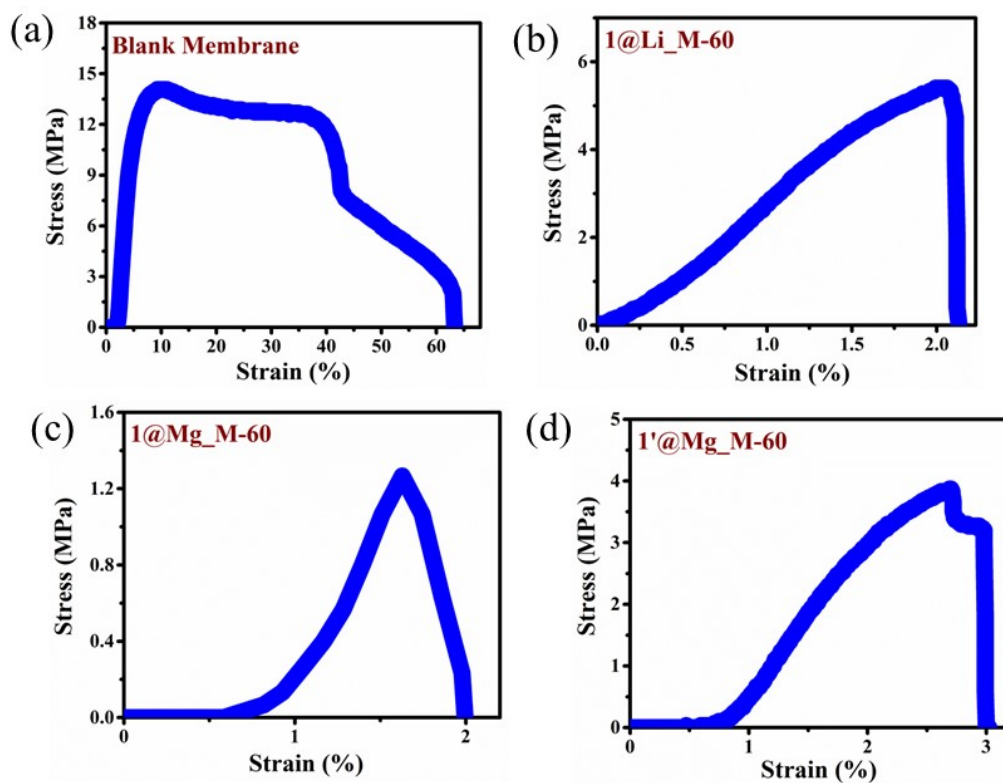


Fig. S35. Stress-strain curve of (a) blank membrane (b)1@Li_M-60 (c)1@Mg_M-60 (d) 1'@Mg_M-60.

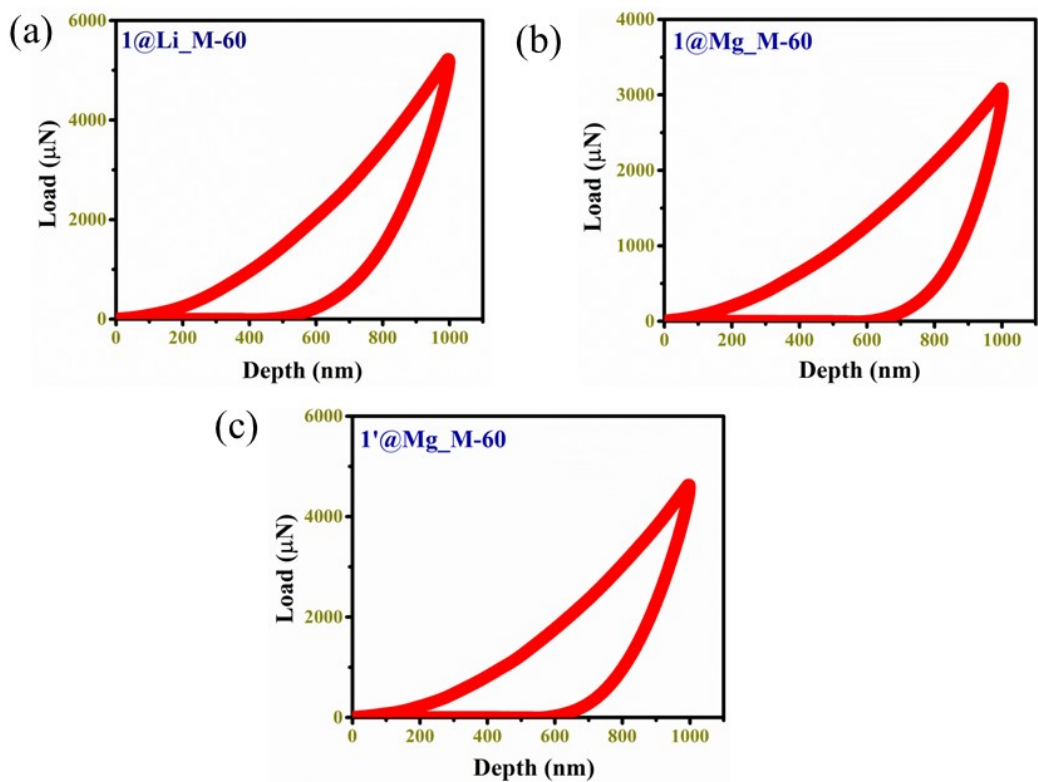


Fig. S36. Load vs depth curve of (a) 1@Li_M-60 (b) 1@Mg_M-60 (c) 1'@Mg_M-60.

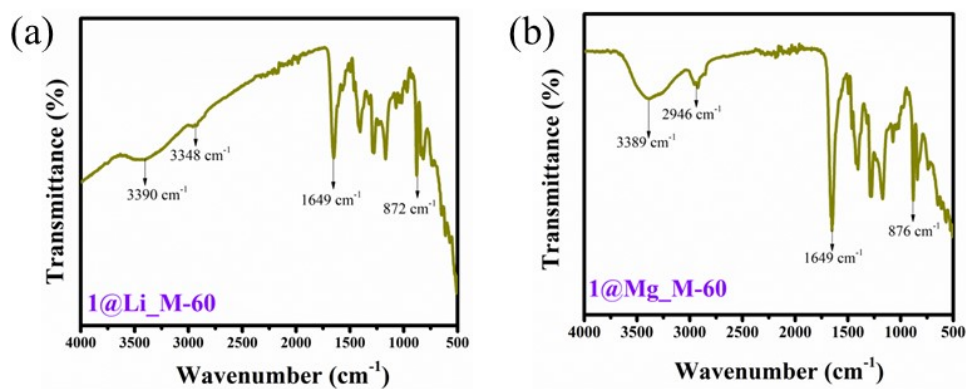


Fig. S37. FTIR plot for 1@Li_M-60 and 1@Mg_M-60.

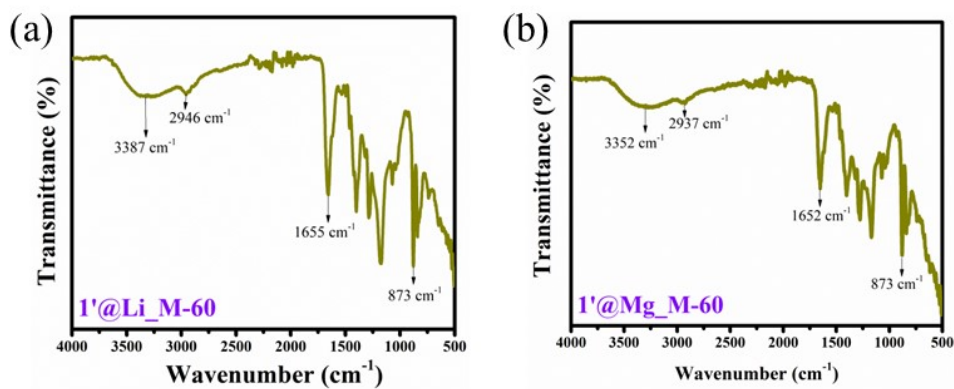


Fig. S38. FTIR plot for 1'@Li_M-60 and 1'@Mg_M-60.

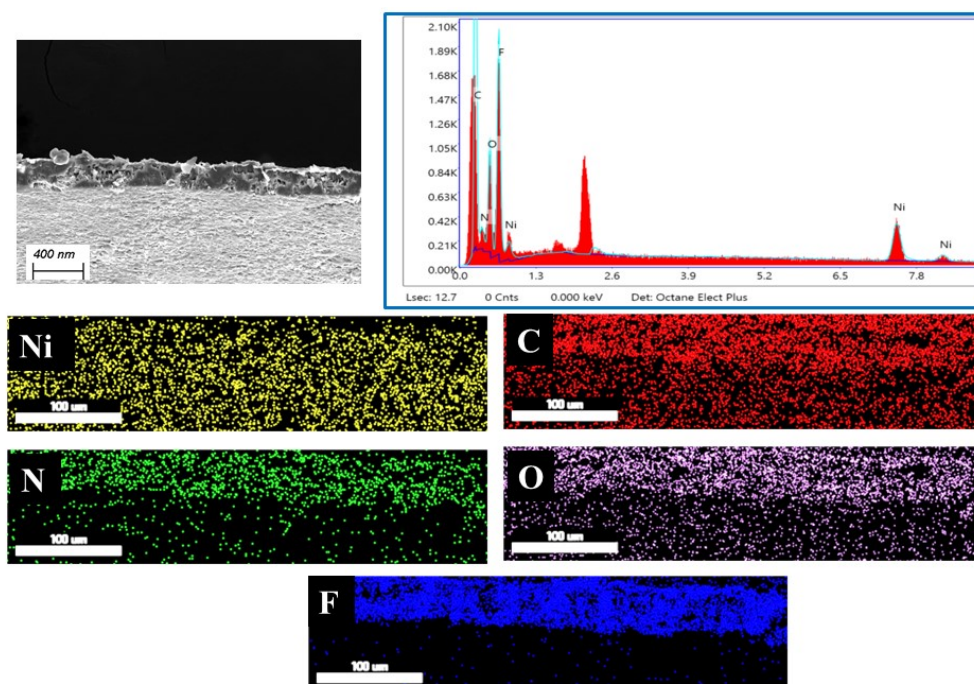


Fig. S39. EDAX and elemental analysis of 1@Li_M-60.

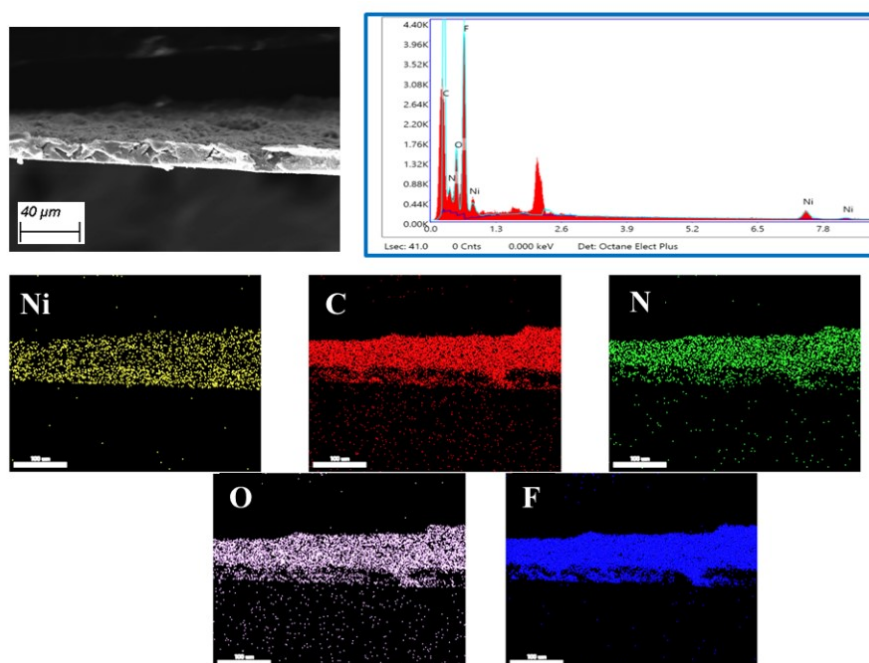


Fig. S40. EDAX and elemental analysis of 1'@Li_M-60.

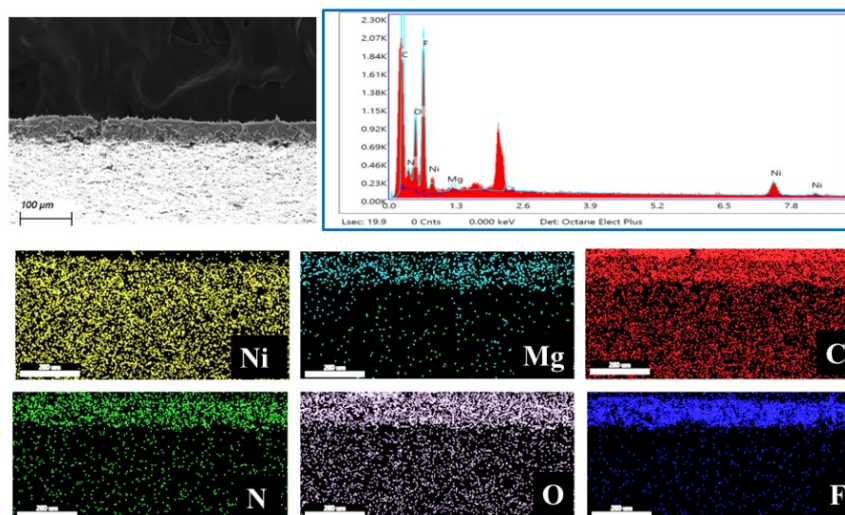


Fig. S41. EDAX and elemental analysis of 1@Mg_M-60.

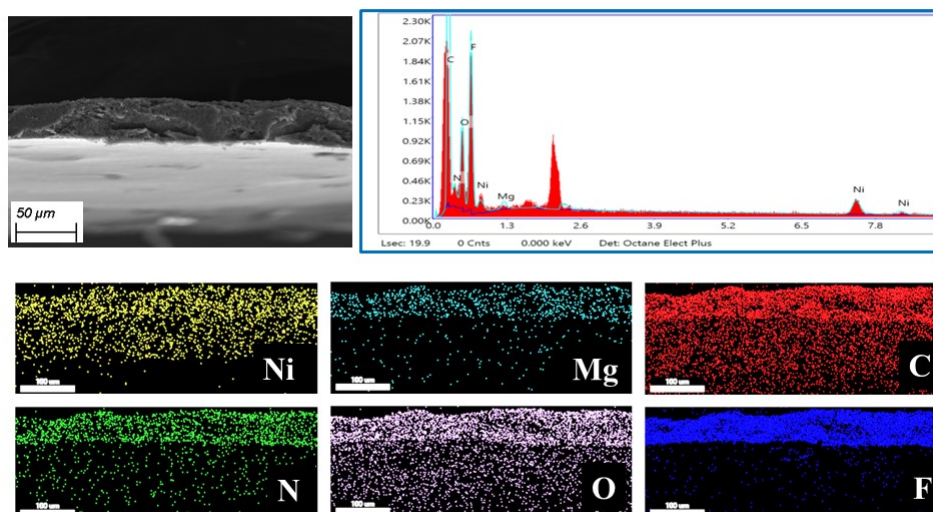


Fig. S42. EDAX and elemental analysis of 1'@Mg_M-60.

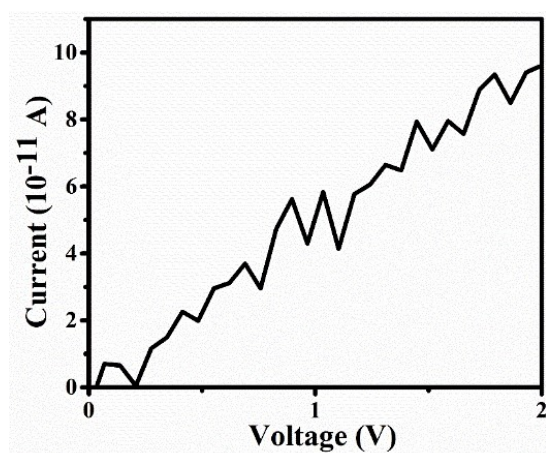


Fig. S43. Current-Voltage (I-V) plots for LiNO₃ embedded PVDF-PVP matrix without Gel material.

Table S2: Conductivity of Mixed-matrix membrane with different loading percentages

Mixed-matrix Membrane	Conductivity value (S cm ⁻¹)
1@Li_M-20	1.07 X 10 ⁻⁶
1@Li_M-40	5.47 X 10 ⁻⁵
1'@Li_M-20	3.01 X 10 ⁻⁵
1'@Li_M-40	5.09 X 10 ⁻³
1@Mg_M-20	1.65 X 10 ⁻⁷
1@Mg_M-40	2.23 X 10 ⁻⁶
1'@Mg_M-20	1.38 X 10 ⁻⁶
1'@Mg_M-40	3.89 X 10 ⁻⁵

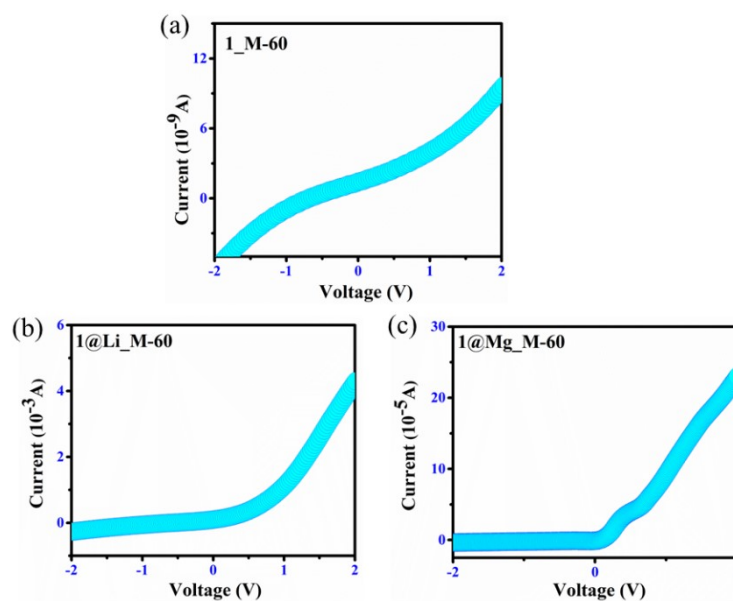


Fig. S44. Current-Voltage (I-V) plots for (a) 1_M-60 (b) 1@Li_M-60 (c) 1@Mg_M-60.

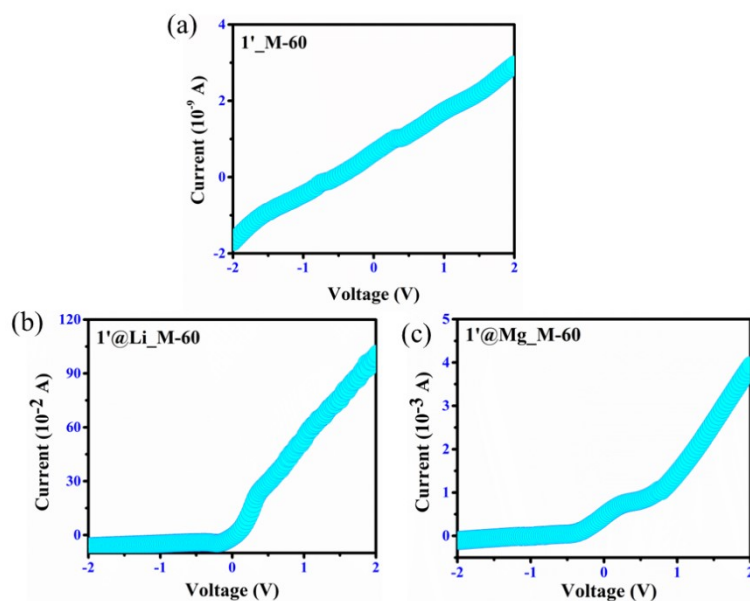


Fig. S45. Current-Voltage (I-V) plots for (a) 1'_M-60 (b) 1'@Li_M-60 (c) 1'@Mg_M-60.

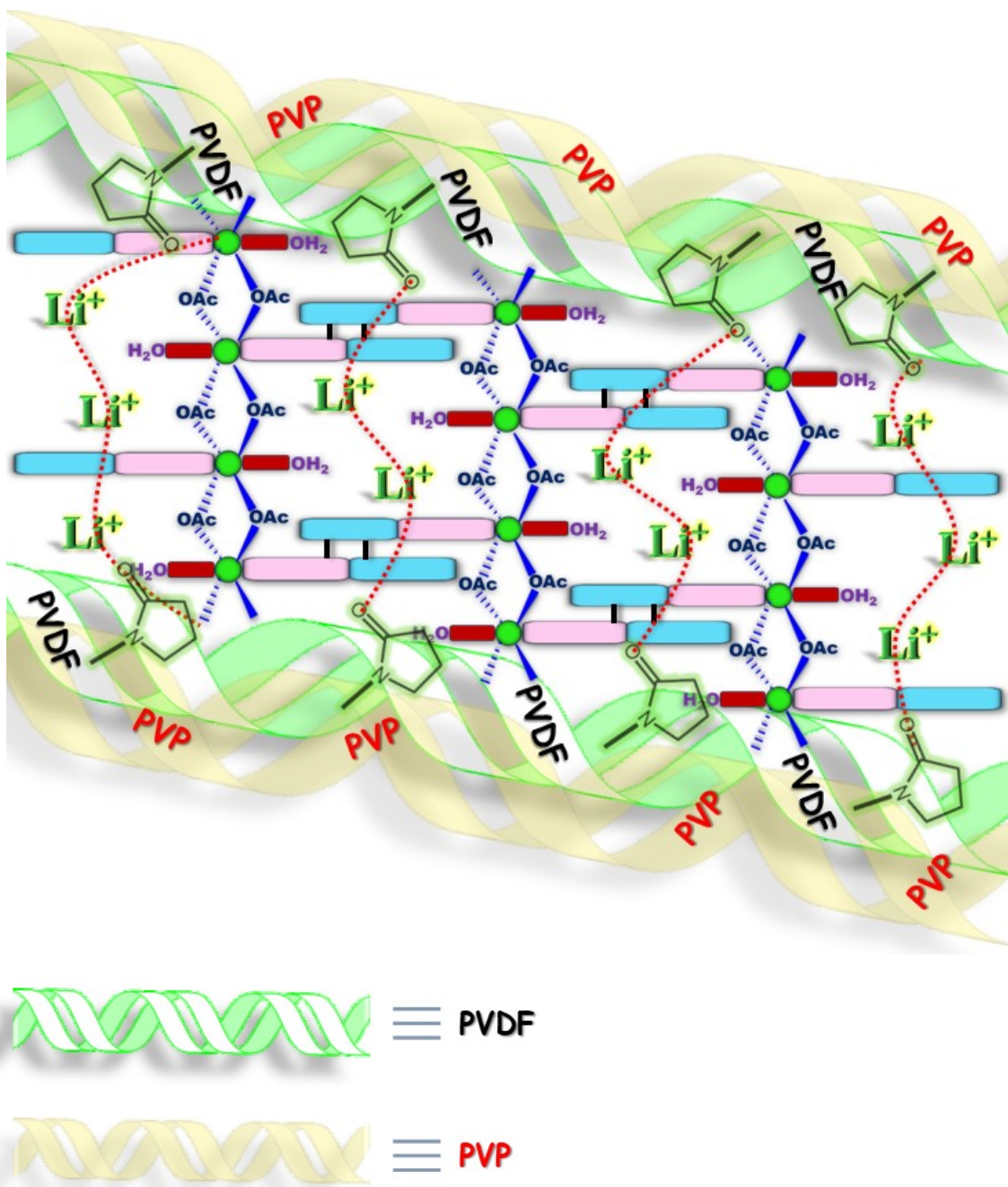


Fig. S46. Probable lithium-ion conduction pathway through mixed-matrix membrane fabrication.

Section S10

Comparison Table

Table S3. Alkali/Alkaline earth metal doped of MOG/MOF-based material

	Materials	σ (S cm ⁻¹)	Ref.
Metal-Organic Gels (MOGs)			
1.	1'@Li_P	5.58 X 10 ⁻⁶	This work
2.	1'@Li_T	1.20 X 10 ⁻⁴	This work
3.	1'@Li_M-60	6.11 X 10 ⁻²	This work
Metal Organic Frameworks (MOFs)			
1.	Mg ₂ (DOBDC)(DMF) ₂	2.1 × 10 ⁻¹⁴	<i>J. Am. Chem. Soc.</i> 2011, 133 , 14522–14525
2.	Mg ₂ (dobdc)@0.05LiBF ₄	1.8 × 10 ⁻⁶	<i>J. Am. Chem. Soc.</i> 2011, 133 , 14522–14525
3.	Mg ₂ (dobdc)@0.06LiO ⁱ Pr	1.2×10 ⁻⁵	<i>J. Am. Chem. Soc.</i> 2011, 133 , 14522–14525
4.	Mg ₂ (dobdc)@0.35LiO ⁱ Pr + 0.25LiBF ₄	3.1×10 ⁻⁴	<i>J. Am. Chem. Soc.</i> 2011, 133 , 14522–14525
5.	MIT-20	10 ⁻¹⁴	<i>J. Am. Chem. Soc.</i> 2017, 139 , 13260–13263
6.	MIT-20-LiCl	1.3 × 10 ⁻⁵	<i>J. Am. Chem. Soc.</i> 2017, 139 , 13260–13263
7.	MIT-20-LiBr	4.4 × 10 ⁻⁵	<i>J. Am. Chem. Soc.</i> 2017, 139 , 13260–13263
8.	MIT-20-LiBF ₄	4.8 × 10 ⁻⁴	<i>J. Am. Chem. Soc.</i> 2017, 139 , 13260–13263
9.	MIT-20-Na	1.8 × 10 ⁻⁵	<i>J. Am. Chem. Soc.</i> 2017, 139 , 13260–13263
10.	MIT-20-Mg	8.8 × 10 ⁻⁷	<i>J. Am. Chem. Soc.</i> 2017, 139 , 13260–13263
11.	Cu ₄ (tppm) ₂ ·0.6CuCl ₂	5.08 × 10 ⁻¹²	<i>J. Am. Chem. Soc.</i> 2019, 141 , 4422–4427
12.	Cu ₄ (tppm) ₂ ·0.6CuCl ₂ @LiCl	2.4 × 10 ⁻⁵	<i>J. Am. Chem. Soc.</i> 2019, 141 , 4422–4427
13.	Cu ₄ (tppm) ₂ ·0.6CuCl ₂ @LiBr	3.2 × 10 ⁻⁵	<i>J. Am. Chem. Soc.</i> 2019, 141 , 4422–4427
14.	Cu ₄ (tppm) ₂ ·0.6CuCl ₂ @LiI	1.1 × 10 ⁻⁴	<i>J. Am. Chem. Soc.</i> 2019, 141 , 4422–4427
15.	Cu ₄ (tppm) ₂ ·0.6CuCl ₂ @MgCl ₂	1.2 × 10 ⁻⁵	<i>J. Am. Chem. Soc.</i> 2019, 141 , 4422–4427
16.	Cu ₄ (tppm) ₂ ·0.6CuCl ₂ @MgBr ₂	1.3 × 10 ⁻⁴	<i>J. Am. Chem. Soc.</i> 2019, 141 , 4422–4427
17.	Li-TMCA	2.98 × 10 ⁻⁸	<i>Chem. Commun.</i> 2020, 56 , 14873–14876
18.	Li-AOIA	5.92 × 10 ⁻⁸	<i>Chem. Commun.</i> 2020, 56 , 14873–14876
19.	Li-AOIA@LiNO ₃	5.53 × 10 ⁻⁶	<i>Chem. Commun.</i> 2020, 56 , 14873–14876
20.	Li-AOIA@LiBF ₄	1.09 × 10 ⁻⁵	<i>Chem. Commun.</i> 2020, 56 , 14873–14876
21.	Li-AOIA@LiCl	2.08 × 10 ⁻⁶	<i>Chem. Commun.</i> 2020, 56 , 14873–14876
22.	Li-AOIA@LiBr	3.42 × 10 ⁻⁶	<i>Chem. Commun.</i> 2020, 56 , 14873–14876
23.	Li-TMCA@LiNO ₃	5.03 × 10 ⁻⁷	<i>Chem. Commun.</i> 2020, 56 , 14873–14876
24.	Li-TMCA@LiBF ₄	2.93 × 10 ⁻⁶	<i>Chem. Commun.</i> 2020, 56 , 14873–14876
25.	HKUST-1@LiClO ₄	3.8 × 10 ⁻⁴	<i>Adv. Mater.</i> 2018, 30 , 1707476

26.	MIL-Al@LiClO ₄	1.22×10^{-3}	<i>Adv. Mater.</i> 2018, 30 , 1707476
27.	MIL-Fe@LiClO ₄	9×10^{-4}	<i>Adv. Mater.</i> 2018, 30 , 1707476
28.	MIL-Cr@LiClO ₄	2.3×10^{-4}	<i>Adv. Mater.</i> 2018, 30 , 1707476
29.	UiO-66@LiClO ₄	1.8×10^{-4}	<i>Adv. Mater.</i> 2018, 30 , 1707476
30.	UiO-67@LiClO ₄	6.5×10^{-4}	<i>Adv. Mater.</i> 2018, 30 , 1707476
31.	Li-BDC@LiClO ₄	4.8×10^{-5}	<i>Chem. Mater.</i> 2023, 35 , 9857–9878
32.	Li-NDC@LiClO ₄	7.49×10^{-5}	<i>Chem. Mater.</i> 2023, 35 , 9857–9878
33.	Li-BPDC@LiClO ₄	1.44×10^{-4}	<i>Chem. Mater.</i> 2023, 35 , 9857–9878
34.	ZIF-67@ZIF-8@LiPF ₆	1.35×10^{-3}	<i>Chem. Commun.</i> , 2020, 56 , 14629–14632
35.	LC-MOFs	1.06×10^{-3}	<i>Nanoscale</i> , 2020, 12 , 6976–6982
36.	SN-ZIF-69	1.37×10^{-4}	<i>J. Mater. Chem. A.</i> , 2022, 10 , 651
37.	UIO-66-SO ₃ Na	3.6×10^{-4}	<i>ACS Appl. Mater. Interfaces.</i> 2021, 13 , 24662–24669
38.	MOF-SN-FEC	7.04×10^{-4}	<i>ACS Appl. Mater. Interfaces.</i> 2021, 13 , 52688
39.	Li-IL@MOF	3.0×10^{-4}	<i>Adv. Mater.</i> , 2017, 30 , 1704436
40.	Al-Td-MOF-1	5.7×10^{-5}	<i>Angew. Chem. Int. Ed.</i> 2018, 57 , 16683–16687
41.	Mg-MOF-74	3.17×10^{-6}	<i>Angew. Chem. Int. Ed.</i> 2019, 58 , 15313–15317
42.	UIO-66_LP	2.9×10^{-3}	<i>Adv. Mater.</i> 2019, 31 , 1808338
43.	UIO-66_LC	1.9×10^{-3}	<i>Adv. Mater.</i> 2019, 31 , 1808338
44.	MIL-121/Na+SE	1.2×10^{-4}	<i>Adv. Energy Mater.</i> 2021, 11 , 2003542
45.	MIL-101 \supset {Mg(TFSI) ₂ } _{1.6}	1.9×10^{-3}	<i>J. Am. Chem. Soc.</i> 2022, 144 , 8669–8675